

Shearigami: Self-Folding via Shear Deformation

Rui Wu, Longqiu Li,* and Zuankai Wang*

Origami and kirigami have become foundations for programmable sheet materials that fold along flexible creases. However, since they are originated from folded paper that allows no in-plane sheet deformation, they suffer from limited folding energy arising from narrow creases, and large varieties of crease patterns are completely non-foldable due to over-constraint. Herein, a new strategy that breaks the limitations of the conventional crease-induced folding kinematics by leveraging a folding effect from in-plane shear deformation of the sheet is reported, and it is referred to as shearigami. It is shown that shearigami extends the realm of foldable structures to include the strictly non-foldable origami patterns such as degree-3 vertices, and the sheet-stored self-folding energy outperforms the crease-stored energy by a potentially two orders of magnitude. Shearigami also inherits the mathematical framework of paper folding and provides a unified view that regards origami and kirigami as two special cases. Herein, self-folding shearigami models are experimentally demonstrated based on previously non-foldable patterns, including artificial muscles with rapid shear-induced extension. The way is paved toward active structures and architected materials with design freedom and self-folding capabilities beyond origami and kirigami.

folding-energy has to be stored in the narrow creases.^[21] Achieving strong self-folding behavior usually requires the introduction of additional deformation modes including stretching of creases,^[22,23] bending outside the creased region,^[24,25] external driving force such as fluidic actuation^[26,27] or mobilization of kirigami cuts.^[28,29]

Meanwhile, the crease-induced folding provides limited design freedom and folding configurations, especially for origami, which is highly susceptible to over-constraint even when the panels were allowed to bend or twist. Large varieties of patterns are completely static in classic origami due to vertex-level constraint that obstructs the folding by geometric interference between adjacent panels. Foldability requires at least four creases to join at each vertex,^[30,31] and degree-4-vertex origami, typically Miura–Ori is therefore the simplest and the most studied origami pattern,^[32–34] while the degree-3 vertex where three creases join together, is completely static.

In addition to vertex-level constraints, origami is also susceptible to global-level constraints when folding is hindered by long-range structural couplings within patterns consisted of foldable vertices.^[35–37] Recent studies have expanded the design space of origami through stretching of creases^[22,23] and out-of-plane deflection of panels,^[38] but still rely on classic crease patterns, and the strictly non-foldable patterns such as degree-3 vertices are still non-foldable. The intriguing task is to find a systematic method to extend the crease-induced paper-folding kinematics, and therefore expand the design space and enhance the self-folding capability, while integrating the abundant design heritage from origami and kirigami.

Here, we create a new strategy that fundamentally breaks the limitations of the crease-induced folding kinematics by leveraging a folding effect driven by in-plane shear deformation of the folded sheet, referred to as shearigami. As mentioned earlier, classic origami is susceptible to being non-foldable due to vertex-level and global-level constraints. In **Figure 1**, we demonstrate shearigami models under both types of constraints but achieve elastic self-foldability. **Figure 1A** demonstrates a paper origami model consists of degree-3 vertices, where the vertex-level constraint makes it strictly non-foldable and fails to fold along the crease pattern although the paper is allowed to bend and twist. To design the shearigami model in **Figure 1B**, we first remove one panel from each of the degree-3 vertices thus relax the vertex-level constraints, and the sheet becomes a kirigami that is passively foldable. We then replace the removed panels with shearing panels constructed from perforated elastic sheet materials (**Figure 2C**). The shearing panels relax the vertex-level

1. Introduction


Transforming the shape of mechanical systems is a timeless subject of engineering design. The recent decade has seen a surge of origami- and kirigami-based systems such as reconfigurable devices,^[1–5] robots,^[6–10] and metastructures^[11–20] that are transformed from sheet materials utilizing the crease-induced folding methodology. However, originated from folded paper, origami and kirigami suppress all in-plane sheet deformation, which fundamentally limits the self-folding capability since all the

R. Wu, L. Li

Key Laboratory of Robotics and System
Harbin Institute of Technology
Harbin 150001, China
E-mail: longqiuli@hit.edu.cn

Z. Wang

Department of Mechanical Engineering
Hong Kong Polytechnic University
Hong Kong SAR 999077, China
E-mail: zuanwang@polyu.edu.hk

 The ORCID identification number(s) for the author(s) of this article can be found under <https://doi.org/10.1002/aisy.202300020>.

© 2023 The Authors. Advanced Intelligent Systems published by Wiley-VCH GmbH. This is an open access article under the terms of the Creative Commons Attribution License, which permits use, distribution and reproduction in any medium, provided the original work is properly cited.

DOI: 10.1002/aisy.202300020

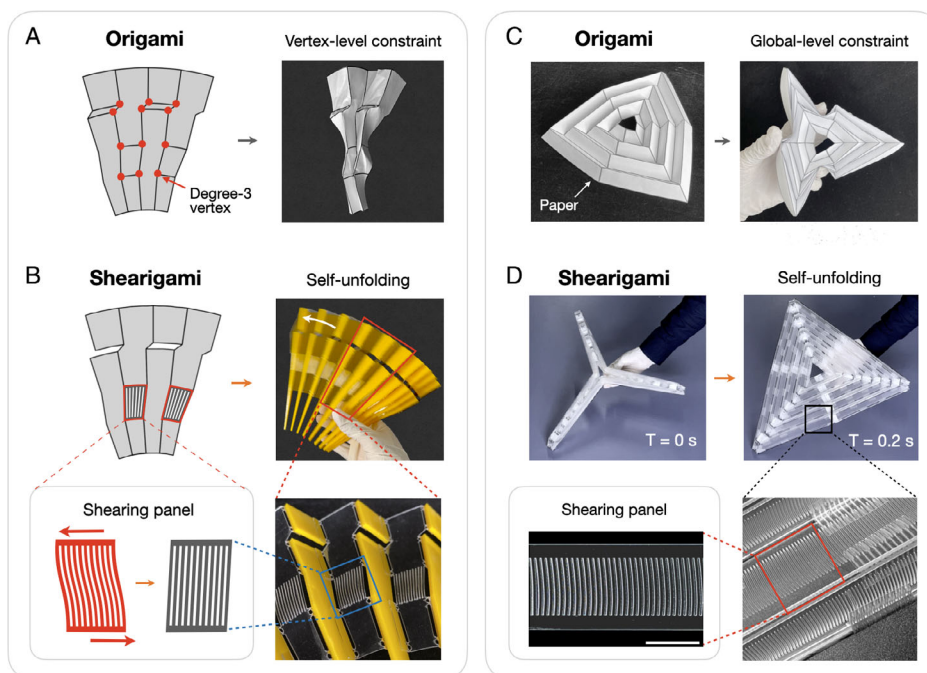


Figure 1. In-plane shear deformation transforms non-foldable origami into self-folding shearigami. A) Origami containing degree-3 vertices is strictly non-foldable due to the in-plane rigidity of paper. The pattern is converted into B) shearigami with panels that elastically accommodate in-plane shear deformation, which not only provides foldability to this pattern, but also enables self-unfolding driven by panel-stored elastic energy, as demonstrated by the model that rapidly unfolds upon release of external constraint (Video S1, Supporting Information). C) A paper origami model that is non-foldable due to global-level interactions in the crease pattern. D) A shearigami model based on the same pattern, but constructed from shearing panels achieves repeatable folding and rapid elastic self-unfolding (Video S2, Supporting Information). Strain energy associated with panel bending, panel twisting, and crease folding is negligible in all models. Scale bar: 10 mm.

constraints through in-plane pure-shear deformation (i.e., a planar distortion that varies the panel apex angles while maintaining the panel side lengths) while generating an energy landscape that drives the unfolding. Although a single shearing panel is sufficient to drive the folding/unfolding of this particular pattern thanks to its fully coupled folding motion (i.e., with a single degree of freedom, as demonstrated by the cognate kirigami pattern in Figure S1B, Supporting Information), the model is designed with multiple shearing panels to guarantee a strong actuation, and the result shows rapid self-unfolding behavior (Video S1, Supporting Information). In addition to vertex-level constraint, Figure 1C demonstrates a paper origami model that is non-foldable due to global-level constraint (the crease pattern is included in Figure S5, Supporting Information). Substituting the paper with shearing panels, the resulting shearigami model is foldable and also self-unfolding (Figure 1D and Video S2, Supporting Information). In the following discussion, we demonstrate through analysis and experiments that the rapid shearigami self-unfolding is driven by strain energy stored within the shearing panels during manual folding process, and such a panel-stored self-folding energy fundamentally outperforms the crease-stored energy in origami and kirigami.

2. Results and Discussion

In Figure 1A,B, we illustrated the characteristics of shearigami through the lens of degree-3 vertex. To further illustrate the role

of in-plane shear deformation and panel-stored energy in shearigami degree-3 vertices, we carried out mechanical analysis and testing using the model shown in Figure 2 and Video S3, Supporting Information. The test model is based on a degree-3 vertex similar to Figure 1B, which has one shearing panel and two rigid panels in each vertex. The shearing panel has parallel slits cut through the thickness (Figure 2C and S2A, Supporting Information), thus when an in-plane shear is applied, it behaves as a group of beams deflected under bending, thereby accommodates the shear deformation in a near pure-shear manner. According to the geometrical analysis (inset of Figure 2B), the shearigami vertex theoretically allows the dihedral angle between the two rigid panels to continuously vary from $\phi = 180^\circ$ (fully-unfolded) to $\phi = 0^\circ$ (flat-folded) at the cost of an apex angle variation (shear deformation) of $\Delta a = -15^\circ$. Since the shearing panel is free of stress at $\phi = 0^\circ$, and a varies monotonically during unfolding, the shearigami exhibits an elastic behavior that tends to fold up as a result of reducing strain energy. In our experiment, the self-folding response from $\phi = 90^\circ$ to $\phi = 150^\circ$ corresponding to an apex angle variation of $\Delta a = -6.5^\circ$ is measured, and the cumulative energy variation closely agrees with the elastic energy associated with panel shear deformation predicted by mechanical analyses and finite-element simulation (Supporting Information), suggesting that the self-folding behavior of this shearigami model is a result of programmed release of strain energy associated with panel shear deformation. To visually illustrate the shearigami kinematics, the design space of

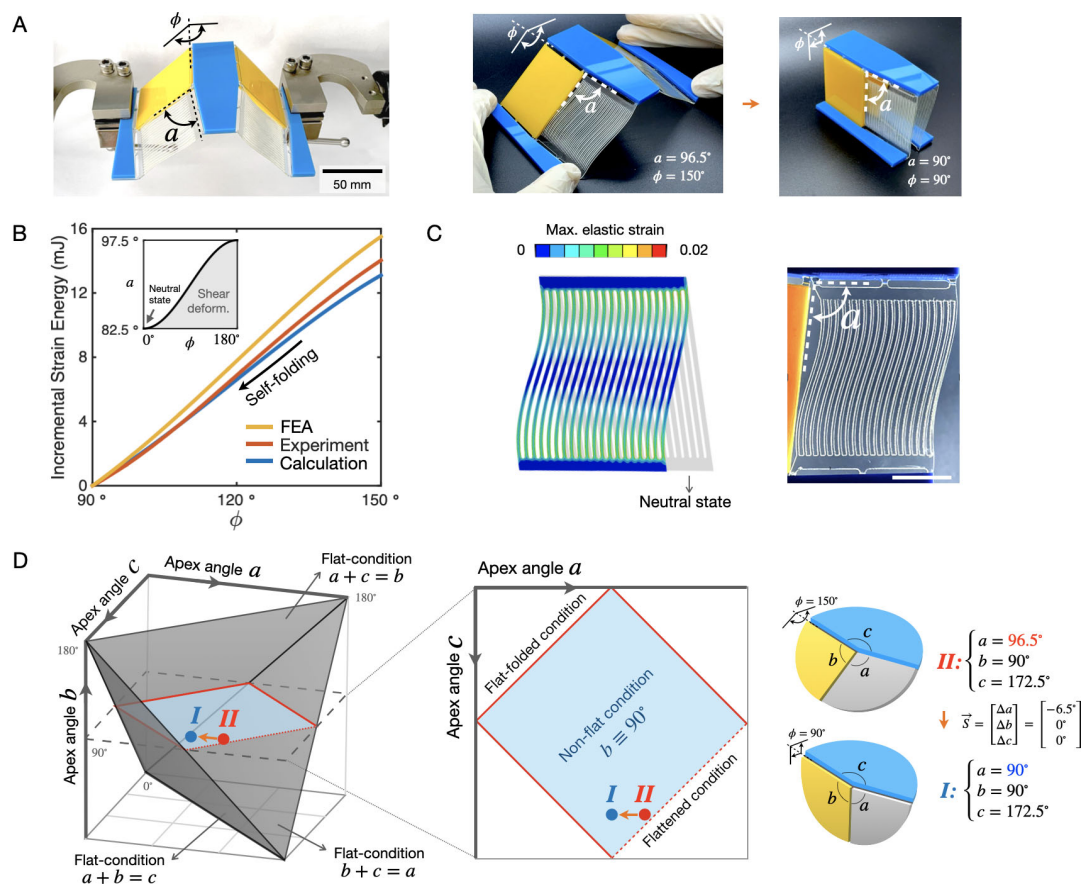


Figure 2. Characterization of the shear-induced self-folding effect of shearigami. A) Test model based on a typical degree-3 vertex that exhibits rapid self-folding behavior (Video S3, Supporting Information). B) Energy associated with shear deformation is used to predict the folding response, with close agreement observed between finite-element simulation, mechanical analyses, and experimental results, inset: variation of panel shear angle during folding. C) Shearing panel design that stores strain energy without plastic yielding to drive the elastic self-folding. Scale bar, 20 mm. D) Design space of degree-3 vertices where all possible apex angle combinations (a, b, c) lie within a tetrahedron volume in Cartesian coordinate, with shearigami transformation denoted by a vector \vec{S} connecting the two folded configurations.

degree-3 vertices is plotted in Figure 2D, where vertex configurations are denoted in Cartesian coordinate by apex angles of the three panels joining at the vertex $[a \ b \ c]$. Any geometrically allowed degree-3 vertices lie within the tetrahedron volume shown in Figure 2D, and the sides of the tetrahedron represents flat configurations (flat-folded and fully flattened). A shearigami folding transformation can be denoted by a vector connecting the vertex configurations before and after folding: $\vec{S} = [\Delta a \ \Delta b \ \Delta c]$, and the elastic strain energy variation depends on the length of this vector: $U \propto |\vec{S}|^2$ (Supporting Information). This allows the folding actuation energy to be designed by tailoring of the folding configurations. As demonstrated in Figure 1D, self-folding of test model transforms the vertex from configuration II to configuration I through a shearigami transformation $\vec{S} = [-6.5^\circ \ 0^\circ \ 0^\circ]$ that determines the self-folding response of this degree-3 vertex.

In addition to the models discussed earlier, we show that shearigami provides flat-foldability to arbitrary shearigami degree-3 vertices (details in Supporting Information). Shearigami flat-foldability can be characterized based on the minimum panel-shearing required to flat-fold a vertex. Assume the three panels joining

at the vertex have initial apex angles of $a, b,$ and c with $a \leq b \leq c < 180^\circ$, and after panel-shearing the apex angles become $a + \Delta a, b + \Delta b,$ and $c + \Delta c,$ respectively. Achieving flat-folding while keeping the shearing to the minimum requires $\Delta a, \Delta b \leq 0,$ and $\Delta c \geq 0,$ and the minimum total panel-shearing required to flat-fold the degree-3 vertex is $\delta = -\Delta a - \Delta b + \Delta c = a + b - c$. Arbitrary degree-3 vertex can be converted into flat-foldable shearigami by introducing a pure-shear δ in one or more panels with any polygonal geometry except triangle, and the minimum strain energy associated with this shearigami transformation, $U_{\min},$ is related to the minimum panel shearing: $U_{\min} \propto \delta^2$. Such a result can be expanded to encompass higher-degree vertices, which is beyond the scope of the present study. It is worth pointing out that the introduction of such a pure-shear deformation that conserves panel side lengths does not require significant modification to the origami and kirigami mathematical model, and more interestingly, they belong to the same extended realm of foldable structures where origami and kirigami can be regarded as two special cases of shearigami (Figure S1, Supporting Information). This implies

a possibility to harness the abundant design heritage of both origami and kirigami to create self-folding shearigami (nevertheless, this can be difficult to implement when considering kirigami patterns with particularly large distortion).

In addition to degree-3 vertices, we have also demonstrated the shearigami model under global-level constraint in Figure 1C,D. The role of panel shear deformation in this model is further investigated here. As illustrated in **Figure 3A**, the pattern consists of six units, each containing nine zigzag-folded panels. When assembled, the six units constrain each other and become a static structure. However, we show that this global-level constraint can be removed by a synchronized shear deformation among the panels. To analyze the folding process, a phenomenological model based on experimentally observed geometrical variation during the folding of the test models is numerically simulated (Figure S4, Supporting Information). The simulated apex angle variation throughout folding is plotted in Figure 3A,B, which suggests that the panels gradually adapt to new folding configurations with a monotonic variation in panel apex angles. The strain energy associated with this panel-shearing process gives rise to the self-unfolding behavior, which can be calculated based

on the panel shear angles. The calculated self-unfolding response of this shearigami model agrees with experimental results (Figure 3C). It is worth noting that the strain energy associated with torsional panel deformation, which has been widely utilized to induce elastic folding effect of origami,^[25,39,40] is two orders of magnitude lower than shear energy according to the numerical analysis, and panel-shearing is the only dominating driving effect in this self-unfolding process (Supporting Information). The effect of shear deformation is further illustrated by the design space shown in Figure 3D, where folding configurations are denoted with respect to edge angle ψ (which describes the extent of folding as defined in Figure 3A) and initial panel apex angle at the fully deployed state (also defined in Figure 3A). The initial panel apex angle is a critical design parameter that determines the foldability of this pattern. According to experiments, patterns with initial apex angles above or equal to 90° are foldable as origami without panel shearing, and such patterns have been studied by other researchers as origami hyper.^[39,41] Patterns with initial apex angles below 90° are non-foldable as origami due to global-level constraint, but can be utilized to design self-unfolding shearigami. When such shearigami is folded under

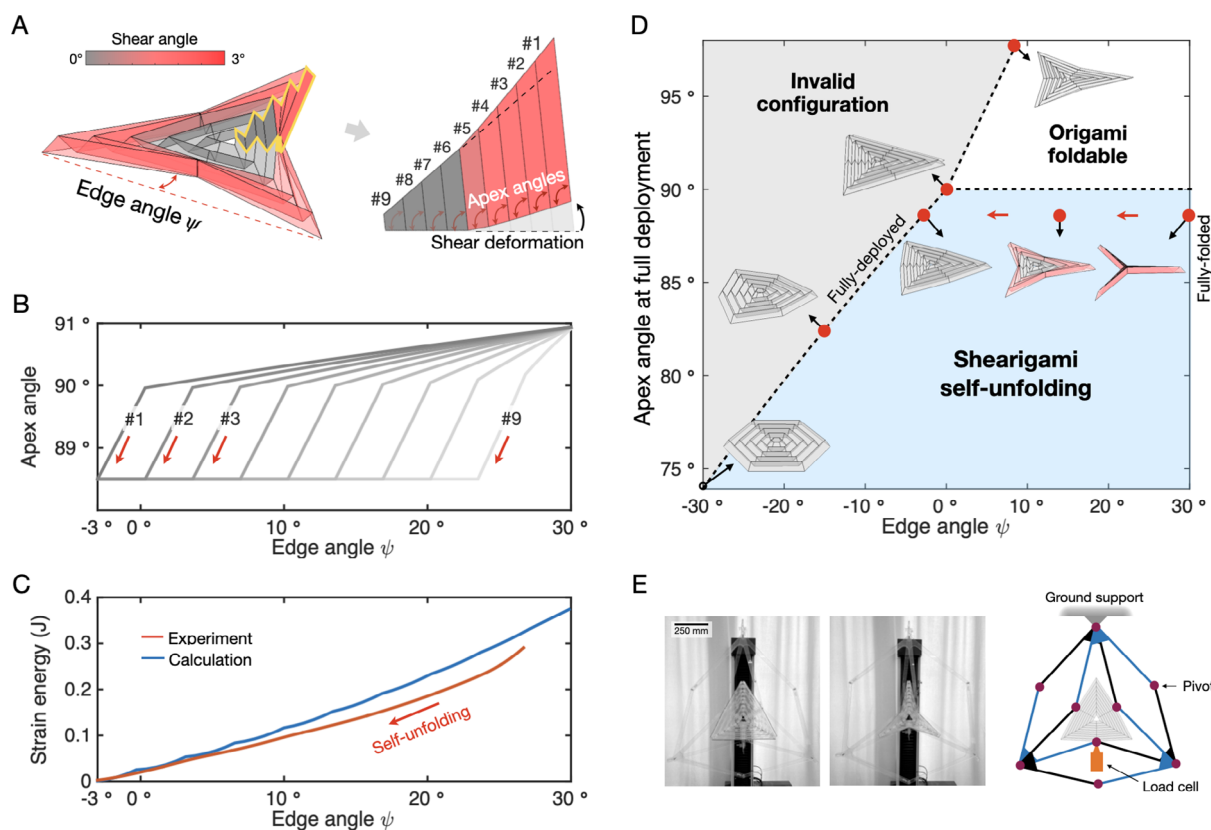


Figure 3. Analysis of the shearigami model under global-level constraint. A) Partially folded geometry predicted by numerical simulation, showing the whole structure as well as one of the six structural units (unfolded), the shear deformation is visually exaggerated by ten times for clarity. B) Simulated variations of panel apex angles in each of the structural units as a result of in plane shear deformation, with the direction of self-unfolding illustrated by the red arrows. C) The self-unfolding behavior can be predicted by calculating the panel-stored strain energy according to the panel apex angles. D) Design space of the shearigami pattern, illustrating that when the initial panel apex angle at full deployment is below 90° , the global-level constraint occurs and the pattern becomes static in origami, but such constraint is utilized by shearigami to achieve self-unfolding driven by panel shear deformation. E) Mechanical test setup, where a test fixture based on planar linkage system is used to realize a synchronized folding motion of the shearigami model.

external driving force, the instantaneous panel apex angles increase to 90° through panel shearing, converting the pattern into an origami-foldable pattern with panel-stored elastic energy. Meanwhile, it is worth noting that in Figure 3B, the panel apex angles reach to above the critical angle of 90° to accommodate panel thickness (the model design for thickness accommodation is included in Supporting Information). The stored energy then drives the self-unfolding when the panel apex angles recover to the initial value. This type of shearigami pattern allows design variations with different structural symmetries, panel shear angles, etc., which we leave for future research.

The panel-induced self-folding (or self-unfolding) of shearigami is fundamentally more effective than the crease-induced folding of origami/kirigami in terms of folding-energy capacity, defined as the overall strain energy variation in one folding cycle. This is because the folding of classic origami/kirigami is driven through rotation (i.e., localized bending) at creases, thus the actuation stress is inevitably concentrated in the narrow crease region, which limits the folding energy. In contrast, folding of shearigami can be actuated from entire panels through uniform shearing, and every panel in a shearigami can be converted into shear actuators. Shearigami therefore provides a possibility toward the ultimate embedded self-folding of sheet materials, where folding-energy capacity is maximized by simultaneous and uniform strain from all of the material within the shearigami structure. To quantify the difference in folding-energy capacity, we carried out theoretical analysis to compare the panel-induced shearigami folding with the crease-induced origami/kirigami folding. In the analysis, we assume the best case scenario for the shearigami, where all of the panels in the shearigami contribute to the folding actuation with synchronized uniform pure shear strain. For the crease-induced folding, we assume 10% of the structural material belongs to the creased regions, which bend simultaneously under plane-strain condition (or infinite crease length). In both cases, we assume the same structural material with linear-elastic homogeneous isotropic behavior throughout the structures, and the structures fold until the material begins to yield according to the von Mises yielding criterion. The total strain energy developed within the structure is then evaluated to characterize the folding-energy capacity of both systems. Details of the analysis can be found in Supporting Information, and the result is reported in Figure 4. It can be seen that with material Poisson's ratio varying between -1 and 0.5 (i.e., the theoretical limit for stable linear-elastic homogeneous isotropic materials), the folding-energy capacity of shearigami increases with Poisson's ratio, and the order of magnitude improvement over crease-induced folding varies between 1.3 and 1.8 (inset of Figure 4). Such a dramatic increase in folding-energy capacity is a combined result from the different volumetric proportion of material that contributes to folding (assumed as 100% and 10% for shearigami panels and origami creases, respectively), and the different stress distribution between panel pure shear and crease bending. It should be noted that origami can perform better than the baseline crease-induced self-folding if the panels were allowed to bend or twist. However, the panel-bending deformation stores a fundamentally lower folding energy than shear (due to the nonuniform stress distribution in bend/twisted panels), and is not considered in this comparison.

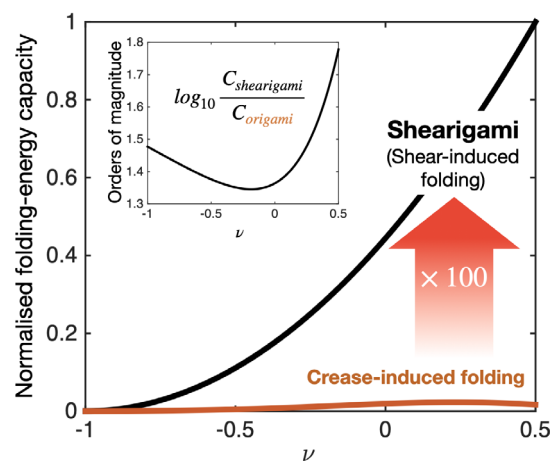


Figure 4. Enhanced folding actuation enabled by shearigami, indicated by theoretical comparison between the maximum strain energy stored through shear-induced and crease-induced folding, calculated with linear-elastic material below yielding point, inset: order-of-magnitude comparison, showing a significantly higher folding-energy capacity by shearigami.

The shear-induced folding transformation in shearigami endows smart actuators with high energy density. Previously, artificial muscles have been developed by harnessing the environmentally activated strain in shape memory materials,^[42,43] electroactive polymers,^[44,45] etc., and the actuation energy density of an artificial muscle is directly determined by the volume fraction of active materials. Shearigami offers a new platform that allows the active materials to achieve near-unit volume fraction in an artificial muscle, which is a radical change over the origami/kirigami system that relies on crease-induced folding. Figure 5A demonstrates a shearigami artificial muscle based on degree-3 vertices that allow panel-induced folding actuation. Driven by shearing panels that occupy over 80% of the total panel area, the demonstration model achieves 20 times linear extension in 40 ms in an elastic manner, while ejecting a projectile that equals its own mass (7 g) to a speed of over 3.5 m s^{-1} (Figure 5B,C and Video S4, Supporting Information), which is equivalent to the speed of a chameleon tongue (Figure 5E).^[46] The shearigami design allows for a designable mechanical response by tailoring of the pattern geometry. Recall that a shearigami folding transformation can be defined as a vector connecting the two vertex configurations before and after folding, and the elastic strain energy variation of the muscle depends on the length of this vector: $U \propto |\vec{S}|^2$, the ejecting speed v of the projectile satisfies $v \propto |\vec{S}|$ according to kinetic energy. This allows the ejection speed to be designed by adjusting the vertex geometry of the muscle, as demonstrated by three sets of tests reported in Figure 5D using test models with different initial panel angles. Finally, it is worth noting that the folding energy density demonstrated in these tests is one order of magnitude lower than the theoretical limit as predicted in Figure 4, mainly because the test models use a shearing panel design based on perforated sheet materials, which has concentrated stress that departs from the ideal uniform shear strain (Figure 2C). Nevertheless, there are abundant possibilities to achieve pure shear through uniform

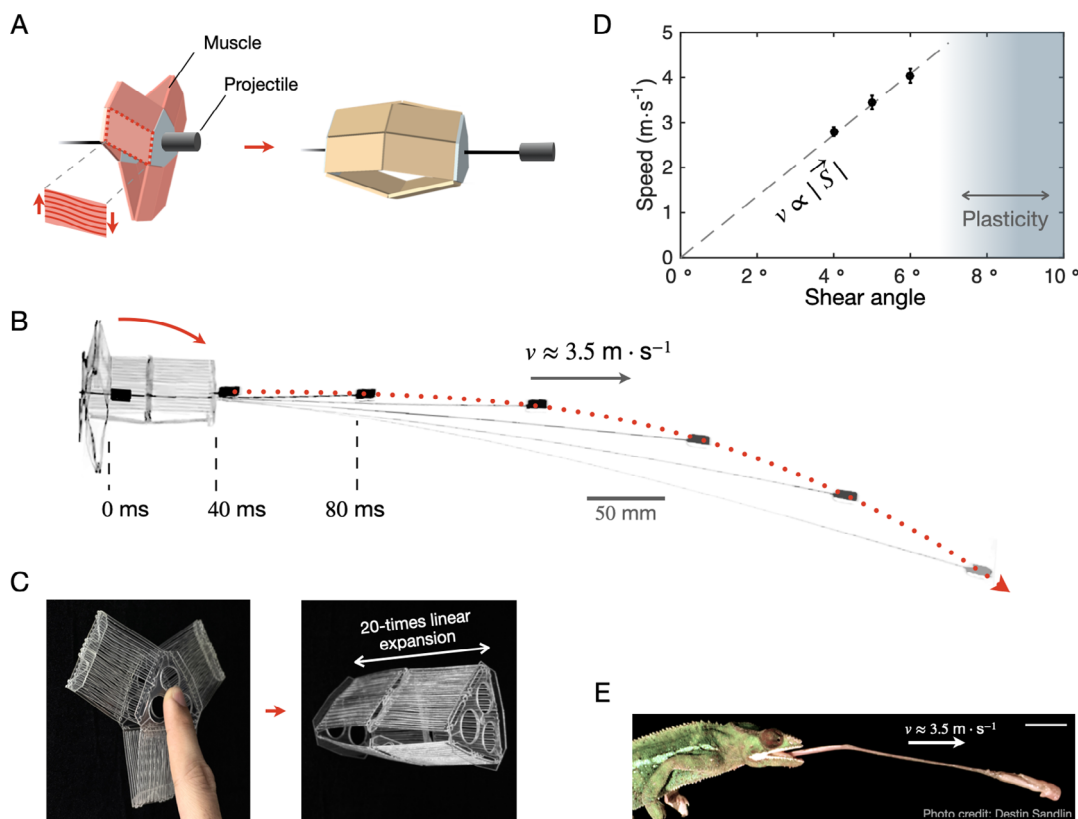


Figure 5. Shearigami artificial muscle based on previously non-foldable degree-3 vertices. A) The muscle design allows elastic energy to be stored within the shearing panels that occupy over 80% of the total panel area. B) Rapid extension of the artificial muscle ejects a projectile equal to its own mass at $3.5 \text{ m} \cdot \text{s}^{-1}$ (Video S4, Supporting Information). C) Close-up view of the demonstration model performing an over-20-times elastic extension. D) Designable projection speed determined by the shearigami transformation \bar{S} . Error bars: range (max–min) of 3 samples. E) The speed of the test projectile is equivalent to chameleon tongue. Scale bar, $\approx 30 \text{ mm}$.

strain using architected material systems,^[47,48] which is beyond the scope of the present study.

3. Conclusion

We introduce shearigami as a new realm of foldable structures that fundamentally expands the crease-dominated folding kinematics and provides a generic perspective toward origami and kirigami. It provides a folding methodology that enables shear-induced self-folding that fundamentally outperforms the conventional crease-induced folding, and novel folding configurations based on strictly non-foldable origami crease patterns (the patterns that are static even when the panels were allowed to bend or twist). Shearigami can be useful in any foldable mechanical systems that benefit from a broader range of attainable configurations and an intrinsic self-folding capability. For example, shearigami metastructures make an ideal platform for self-folding devices based on smart materials^[49,50] with active panel shear deformation, and new types of smart mechanical transducers such as energy harvesters^[51,52] can be designed with transducer materials embedded in the uniformly sheared panels to achieve effective energy conversion. With shearigami, we anticipate to bring new life to the timeless art of paper folding.

4. Experimental Section

Fabrication of Shearigami Demonstration Models: All shearing panels were made from polyethylene terephthalate (PET) polymer sheets with 0.8 mm thickness. According to our testing, the PET sheet material had a Young's modulus of 1.13 GPa and yield strain of over 2.5%. The shearing panel made from PET could elastically accommodate a 15° shear without plasticity, according to finite-element analysis (Figure 2C). Colored acrylic sheets with 3 mm thickness were also used in some of the rigid panels. To fabricate the shearigami model in Figure 1B and 2, a computer numerical control laser cutter was used to perforate and cut individual panels from the sheet materials, and the acrylic sheets were then laminated above the PET sheet through UV curable adhesive to achieve the rigid panel behavior. For the model in Figure 1D, 3M Filament Tape 8934 (glass-fiber-reinforced pressure-sensitive tape) was used to join the panels together. The tape induced negligible resistance to crease folding but high resistance to crease opening. The model in Figure 1D also had extra panels to accommodate the thickness of the sheet material during flat-folding (more details are included in Figure S3, Supporting Information). For the artificial muscle, the sheet material was laser-cut into patterns containing both the shearing panels and the rigid panels connected through creases. The creases were folded for over 100 cycles before the tests to guarantee a minimum rotational resistance and a repeatable mechanical response.

Mechanical Testing: All tests on shearigami models were carried out on an Instron machine with a 50 N load cell at a $200 \text{ mm} \cdot \text{s}^{-1}$ crosshead speed. During the test shown in Figure 3E, folding was driven by equal

inward displacement applied on the three mid-edge points of the test model through a customized test fixture. The test fixture was a planar linkage system that transformed the linear crosshead motion into the three mid-edge displacement, and transferred the folding force to the load cell. Ball bearings were used in the pivots to remove the effect of friction. Strain energy was then calculated from the force and crosshead displacement data while subtracting the effect of gravity, and the edge angle ψ was evaluated from the crosshead displacement using simple geometry.

Supporting Information

Supporting Information is available from the Wiley Online Library or from the author.

Acknowledgements

This research was supported by the National Natural Science Foundation of China (Grant nos. 52005127 and 52125505), Key-Area Research and Development Program of Guangdong Province, China (Grant no. 2020B090923003), and Innovation and Technology Fund (Grant no. GHP/021/19SZ). We especially thank C. Soutis for the valuable discussions.

Conflict of Interest

The authors declare no conflict of interest.

Data Availability Statement

The data that support the findings of this study are available from the corresponding author upon reasonable request.

Keywords

artificial muscles, foldability, mechanical metamaterials, metasheets, self folding

Received: January 31, 2023

Revised: March 9, 2023

Published online: May 24, 2023

- [1] L. H. Dudte, E. Vouga, T. Tachi, L. Mahadevan, *Nat. Mater.* **2016**, *15*, 583.
- [2] Y. Chen, R. Peng, Z. You, *Science* **2015**, *349*, 396.
- [3] E. T. Filipov, T. Tachi, G. H. Paulino, *Proc. Natl. Acad. Sci.* **2015**, *112*, 12321.
- [4] S. Lim, H. Luan, S. Zhao, Y. Lee, Y. Zhang, Y. Huang, J. A. Rogers, J.-H. Ahn, *Adv. Mater.* **2020**, *32*, 2001303.
- [5] T. A. Evans, R. J. Lang, S. P. Magleby, L. L. Howell, *Roy. Soc. Open Sci.* **2015**, *2*, 150067.
- [6] Z. Jiao, C. Zhang, W. Wang, M. Pan, H. Yang, J. Zou, *Adv. Sci.* **2019**, *6*, 1901371.
- [7] S.-J. Kim, D.-Y. Lee, G.-P. Jung, K.-J. Cho, *Sci. Robot.* **2018**, *3*, eaar2915.
- [8] D.-Y. Lee, J.-K. Kim, C.-Y. Sohn, J.-M. Heo, K.-J. Cho, *Sci. Robot.* **2021**, *6*, eaab0201.
- [9] S. Jiang, J. Liu, W. Xiong, Z. Yang, L. Yin, K. Li, Y. Huang, *Adv. Mater.* **2022**, 2204091.
- [10] S. Felton, M. Tolley, E. Demaine, D. Rus, R. Wood, *Science* **2014**, *345*, 644.
- [11] M. Meloni, J. Cai, Q. Zhang, D. Sang-Hoon Lee, M. Li, R. Ma, T. E. Parashkevov, J. Feng, *Adv. Sci.* **2021**, *8*, 2000636.
- [12] J. L. Silverberg, A. A. Evans, L. McLeod, R. C. Hayward, T. Hull, C. D. Santangelo, I. Cohen, *Science* **2014**, *345*, 647.
- [13] J. T. Overvelde, T. A. De Jong, Y. Shevchenko, S. A. Becerra, G. M. Whitesides, J. C. Weaver, C. Hoberman, K. Bertoldi, *Nat. Commun.* **2016**, *7*, 10929.
- [14] S. Babaei, J. T. Overvelde, E. R. Chen, V. Tournat, K. Bertoldi, *Sci. Adv.* **2016**, *2*, 1601019.
- [15] Z. Wang, L. Jing, K. Yao, Y. Yang, B. Zheng, C. M. Soukoulis, H. Chen, Y. Liu, *Adv. Mater.* **2017**, *29*, 1700412.
- [16] H. Fang, S.-C. A. Chu, Y. Xia, K.-W. Wang, *Adv. Mater.* **2018**, *30*, 1706311.
- [17] J. Tao, H. Khosravi, V. Deshpande, S. Li, *Adv. Sci.* **2022**, 2204733.
- [18] X. Zhang, J. Ma, M. Li, Z. You, X. Wang, Y. Luo, K. Ma, Y. Chen, *Proc. Natl. Acad. Sci.* **2022**, *119*, 2117649119.
- [19] A. Jamalimehr, M. Mirzajanzadeh, A. Akbarzadeh, D. Pasini, *Nat. Commun.* **2022**, *13*, 1816.
- [20] X. Liu, J. M. Gattas, Y. Chen, *Sci. Rep.* **2016**, *6*, 36883.
- [21] T. van Manen, V. M. Dehabadi, M. C. Saldívar, M. J. Mirzaali, A. A. Zadpoor, *Commun. Mater.* **2022**, *3*, 43.
- [22] J. A. Faber, A. F. Arrieta, A. R. Studart, *Science* **2018**, *359*, 1386.
- [23] S. Mintchev, J. Shintake, D. Floreano, *Sci. Robot.* **2018**, *3*, eaau0275.
- [24] N. P. Bende, A. A. Evans, S. Innes-Gold, L. A. Marin, I. Cohen, R. C. Hayward, C. D. Santangelo, *Proc. Natl. Acad. Sci.* **2015**, *112*, 11175.
- [25] J. L. Silverberg, J.-H. Na, A. A. Evans, B. Liu, T. C. Hull, C. D. Santangelo, R. J. Lang, R. C. Hayward, I. Cohen, *Nat. Mater.* **2015**, *14*, 389.
- [26] D. Melancon, B. Gorissen, C. J. García-Mora, C. Hoberman, K. Bertoldi, *Nature* **2021**, *592*, 545.
- [27] S. Li, J. J. Stampfli, H. J. Xu, E. Malkin, E. V. Diaz, D. Rus, R. J. Wood, in *Int. Conf. on Robotics and Automation*, IEEE, Piscataway NJ **2019**, pp. 7401–7408.
- [28] T. van Manen, S. Janbaz, M. Ganjian, A. A. Zadpoor, *Mater. Today* **2020**, *32*, 59.
- [29] J. Cui, F. R. Poblete, Y. Zhu, *Adv. Funct. Mater.* **2018**, *28*, 1802768.
- [30] M. Stern, M. B. Pinson, A. Murugan, *Phys. Rev. X* **2017**, *7*, 041070.
- [31] L. Zimmermann, K. Shea, T. Stanković, *J. Mech. Robot.* **2020**, *12*, 011020.
- [32] K. Miura, Method of Packaging and Deployment of Large Membranes in Space, The Institute of Space and Astronautical Science Report, The Institute of Space and Astronautical Science, Sagami-hara, Kanagawa, Japan **1985**, pp. 1–9.
- [33] J. M. Gattas, W. Wu, Z. You, *J. Mech. Des.* **2013**, *135*, 111011.
- [34] H. Fang, S. Li, K. Wang, *Proc. Roy. Soc. A: Math. Phys. Eng. Sci.* **2016**, *472*, 20160682.
- [35] M. Bern, B. Hayes, in *Proc. of the Seventh Annual ACM-SIAM Symp. on Discrete Algorithms*, Vol 96, Soc for Industrial and Applied Mathematics, Philadelphia pp. 175–183.
- [36] A. A. Evans, J. L. Silverberg, C. D. Santangelo, *Phys. Rev. E* **2015**, *92*, 013205.
- [37] B. Liu, J. L. Silverberg, A. A. Evans, C. D. Santangelo, R. J. Lang, T. C. Hull, I. Cohen, *Nat. Phys.* **2018**, *14*, 811.
- [38] W. Kim, J. Byun, J.-K. Kim, W.-Y. Choi, K. Jakobsen, J. Jakobsen, D.-Y. Lee, K.-J. Cho, *Sci. Robot.* **2019**, *4*, eaay3493.
- [39] K. Liu, T. Tachi, G. H. Paulino, *Nat. Commun.* **2019**, *10*, 4238.
- [40] H. Yasuda, Y. Miyazawa, E. G. Charalampidis, C. Chong, P. G. Kevrekidis, J. Yang, *Sci. Adv.* **2019**, *5*, eaau2835.
- [41] E. Filipov, M. Redoutey, *Extreme Mech. Lett.* **2018**, *25*, 16.
- [42] A. Lendlein, H. Jiang, O. Jünger, R. Langer, *Nature* **2005**, *434*, 879.

- [43] A. Lendlein, *Sci. Robot.* **2018**, 3, eaat9090.
- [44] T. H. Ware, M. E. McConney, J. J. Wie, V. P. Tondiglia, T. J. White, *Science* **2015**, 347, 982.
- [45] T. J. White, D. J. Broer, *Nat. Mater.* **2015**, 14, 1087.
- [46] C. V. Anderson, *Sci. Rep.* **2016**, 6, 18625.
- [47] R. Wu, J. Sun, Z. Chang, R. Bai, J. Leng, *J. Intell. Mater. Syst. Struct.* **2015**, 26, 352.
- [48] Z. D. Jastrzebski, *Nature and Properties of Engineering Materials*, John Wiley and Sons, Inc., New York **1976**.
- [49] B. Bircan, M. Z. Miskin, R. J. Lang, M. C. Cao, K. J. Dorsey, M. G. Salim, W. Wang, D. A. Muller, P. L. McEuen, I. Cohen, *Nano Lett.* **2020**, 20, 4850.
- [50] J.-H. Na, A. A. Evans, J. Bae, M. C. Chiappelli, C. D. Santangelo, R. J. Lang, T. C. Hull, R. C. Hayward, *Adv. Mater.* **2015**, 27, 79.
- [51] Z. L. Wang, T. Jiang, L. Xu, *Nano Energy* **2017**, 39, 9.
- [52] A. Ahmed, I. Hassan, M. F. El-Kady, A. Radhi, C. K. Jeong, P. R. Selvaganapathy, J. Zu, S. Ren, Q. Wang, R. B. Kaner, *Adv. Sci.* **2019**, 6, 1802230.